Tunable Stable Levitation Based on Casimir Interaction between Nanostructures

Xianglei Liu and Zhuomin M. Zhang

Phys. Rev. Applied **5**, 034004 — Published 9 March 2016

DOI: 10.1103/PhysRevApplied.5.034004

Reference reformatted February 18, 2016
Revision submitted to **Phys. Rev. Applied** on January 17, 2016
Original submitted to *PRA* on August 15, 2015 (transferred to *Phys. Rev. Applied*)

Tunable stable levitation based on Casimir interaction between nanostructures

Xianglei Liu and Zhuomin M. Zhang[1]

George W. Woodruff School of Mechanical Engineering
Georgia Institute of Technology, Atlanta, GA 30332, USA

Abstract

Quantum levitation enabled by repulsive Casimir force has been a desire due to the potential exciting applications in passive-suspension devices and frictionless bearings. In this paper, dynamically tunable stable levitation is theoretically demonstrated based on the configuration of dissimilar gratings separated by an intervening fluid using exact scattering theory. The levitation position is insensitive to temperature variations and can be actively tuned by adjusting the lateral displacement between the two gratings. This work paves a way toward applying quantum Casimir interactions into macroscopic mechanical devices working in a noncontact and low-friction environment for controlling the position or transducing lateral movement into vertical displacement at the nanoscale.

PACS numbers: 42.50.Lc, 03.70.+k, 85.85.+j

[1] Corresponding author: Telephone: (01) 404-385-4225; E-mail: zhuomin.zhang@me.gatech.edu.

I. INTRODUCTION

Since being discovered in 1948 [1], the Casimir effect has attracted intensive attention especially in the last two decades when it has gone through significant progresses benefiting from current nanofabrication techniques and development of new calculation methods [2-8]. Recent experimental setups and computational capabilities are able to consider complex geometries beyond simple planar configurations [9-20], two-dimensional (2D) materials [21-26], and effects of thermal fluctuations [27-32]. Nevertheless, the basic mechanism of these different Casimir interactions is the same, a dispersion force induced by quantum and thermal fluctuations. The changing of quantized electromagnetic field in the vacuum gap due to presence of boundary conditions is attributed to the usual attraction force between neutral objects; otherwise no force will exist given that there are no real photons (0 K) or fields according to classical electrodynamics. Despite its quantum nature, the Casimir interaction is a macroscopic phenomenon and has played an important role in condensed matter physics, particle physics, as well as cosmology [2]. The attractive Casimir force per unit area between two perfect metals at 0 K is given as $F_{\mathrm{C}} = \pi^2 \hbar c \big/ \left(240 d^4\right)$, where d is the gap spacing, $\hbar$ is reduced Planck constant, c is the speed of light in vacuum [1]. Its magnitude increases quickly with decreasing gap spacing, and the corresponding pressure exerted is even larger than atmospheric pressure at d = 10 nm. This nontrivial long-range interaction will cause the malfunctioning of microelectromechanical systems (MEMS) and nanoelectromechanical systems (NEMS) due to the induced stiction and friction problems. As a result, it may impede on Moore's law, which says that the packing density of transistors doubles approximately every two years.

The desire of overcoming the Casimir stiction has been one of the major driving forces for realizing repulsive force. Magnetic materials were introduced to achieve the Casimir

repulsion through the vacuum gap [33, 34]. However, both these cases are based on nonphysical assumptions since infinite permeability is used by Boyer [33] and the independence of frequency for both permittivity and permeability is employed by Kenneth et al. [34]. Indeed, materials supporting non-unity permeability in the optical region which usually has the dominant contribution to the Casimir force do not exist in nature. This is because the interaction of materials with the magnetic field of electromagnetic waves is weak especially for short wavelengths due to the small value of the Sommerfeld fine-structure constant. Fortunately, artificial metamaterials with subwavelength unit cells such as split-ring resonators have been both theoretically and experimentally demonstrated to support strong magnetic responses. Based on the effective medium theory (EMT), both metamaterials supporting effective magnetic resonances and chiral materials with strong anisotropy have been claimed to induce repulsive Casimir force [35-40]. Nevertheless, the validity of EMT at small gap spacing is questionable [41], and exact calculations have recently proved effects of chirality to be small [42]. Therefore, achieving repulsive force in vacuum is still very challenging, although it has been demonstrated for ferromagnetic dielectrics [43] or in some situations out of thermal equilibrium [44]. Besides, very recent theories have ascertained that achieving stable levitation in vacuum to be impossible since Casimir free energy in vacuum for nonmagnetic materials has no minima [45-47].

Replacing the vacuum with an intervening fluid helps realize repulsion force, and stable levitation has been demonstrated based on dissimilar bulk substrates, changing the density of charge carriers by laser pulses, and more recently thin-film coatings [48-55]. However, the stable levitation is not actively tunable. The present study theoretically demonstrates stable suspension supporting on-site tunability by using one-dimensional (1D) gratings. The methods employed in this work are briefly described in Sec. II, including exact scattering theory, proximity force

approximation (PFA), and general Lifshitz's theory. The requirements of stable levitation and limitations of current techniques of employing bulks and thin films for quantum levitation are discussed in Sec. III. Tunable stable levitation based on nanostructures is demonstrated in Sec. IV. The effects of temperature and gravity are discussed in Sec. V, followed by a conclusion.

II. APPROACHES TO CHARACTERIZE CASIMIR INTERACTION BETWEEN NANOSTRUCTURES

The configuration of two patterned plates immersed in the fluid bromobenzene with a gap spacing of d is illustrated in Fig. 1. In order to make the analysis simpler, the grating period (P) and width (W) are assumed to be the same for both the top Si grating and the bottom Teflon grating, which have different depths of H_1 and H_2, respectively. The associated substrates are bulk intrinsic Si for both gratings, and the lateral shift between the two gratings is L ($0 \le L < P$ with $L = 0$ for aligned case). The Casimir force in the z direction per unit area at thermal equilibrium conditions with a finite temperature of T can be calculated using exact scattering theory based on the following expression [10, 13, 28]:

$$F = 2\pi k_B T \sum_{n=0}^{\infty}{}' \int_{-\infty}^{\infty}\int_{-\pi/P}^{\pi/P} \mathrm{tr}\left[(\mathbf{1}-\mathbf{M}_n)^{-1}\partial_z \mathbf{M}_n\right] dk_x dk_y \tag{1}$$

where the prime in the summation operator means the $n = 0$ term should be taken with a factor of 0.5. Both quantum and thermal fluctuations are taken into account, so the summation should be exerted over Matsubara frequencies $i\omega_n = i2\pi n k_B T/\hbar$, where n is an integer ranging from 0 to infinity and k_B is the Boltzmann constant. The default temperature T is set to be 300 K, and the temperature dependence will be discussed later. Matrix $\mathbf{M}_n$ can be described by reflection

coefficients $\mathbf{R}_1$ and $\mathbf{R}_2$ at Matsubara frequencies [28], which consider all possible polarization states and are obtained by using the rigorous coupled-wave analysis (RCWA) for specified k_x and k_y values [28, 56-59]. The integration range of k_x is from $-\pi/P$ to π/P rather than from $-\infty$ to ∞ because all the modes are folded into the first Brillouin zone due to the periodicity in the x direction. It takes about one hour to calculate the Casimir force between the two gratings with specific geometric parameters at a certain gap distance using a dual eight core XEON E5-2687W workstation.

One simple and fast approximate method for predicting the Casimir interaction between 1D gratings is the well-known PFA. This method assumes that the Casimir force is additive and can be obtained as weighted average of plane-plane configurations at different gap distances. Assuming $W/P \le 0.5$, the Casimir force by PFA can be written as

$$F_{PFA} = \begin{cases} \dfrac{W-L}{P}F_d^{\mathrm{Te}} + \dfrac{L}{P}F_{d+H_1}^{\mathrm{Te}} + \dfrac{L}{P}F_{d+H_2}^{\mathrm{Si}} + \dfrac{P-W-L}{P}F_{d+H_1+H_2}^{\mathrm{Si}}, & L \le W \\ \dfrac{W}{P}F_{d+H_1}^{\mathrm{Te}} + \dfrac{W}{P}F_{d+H_2}^{\mathrm{Te}} + \dfrac{P-2W}{P}F_{d+H_1+H_2}^{\mathrm{Si}}, & W < L \le P-W \\ \dfrac{W+L-P}{P}F_d^{\mathrm{Te}} + \dfrac{(P-L)}{P}F_{d+H_1}^{\mathrm{Te}} + \dfrac{(P-L)}{P}F_{d+H_2}^{\mathrm{Si}} + \dfrac{L-W}{P}F_{d+H_1+H_2}^{\mathrm{Si}}, & L > P-W \end{cases} \quad (2)$$

Superscripts "Si" and "Te" represent the plane configuration of Si-bromobenzene-Si and Si-bromobenzene-Teflon-Si, respectively. Subscripts d, $d+H_1$, $d+H_2$, and $d+H_1+H_2$ denote different gap distances.

The Casimir force per unit area between isotropic substrates separated by a fluid can be described by the general Lifshitz's theory as [60-62]

$$F_{\mathrm{plane}} = \frac{k_B T}{\pi}\sum_{n=0}^{\infty}{}' \int_0^{\infty} k_{zn}\left(\frac{r_1^{\mathrm{s}} r_2^{\mathrm{s}} e^{-2k_{zn}d}}{1-r_1^{\mathrm{s}} r_2^{\mathrm{s}} e^{-2k_{zn}d}} + \frac{r_1^{\mathrm{p}} r_2^{\mathrm{p}} e^{-2k_{zn}d}}{1-r_1^{\mathrm{p}} r_2^{\mathrm{p}} e^{-2k_{zn}d}}\right)\beta d\beta \quad (3)$$

where $\beta = \sqrt{k_x^2 + k_y^2}$ is the tangential wavevector, $k_{zn} = \sqrt{\varepsilon_f \, \omega_n^2 / c^2 + \beta^2}$ is the vertical wavevector of the intervening fluid, subscripts "s" and "p" represent *s*- and *p*-polarization waves. r_1 and r_2 are the Fresnel reflection coefficients evaluated at Matsubara frequencies for the fluid interface with substrate 1 and 2, respectively. Equation (3) holds if the substrate is a three-layer structure provided the reflection coefficient is obtained using Airy's formula [63].

III. STABLE LEVITATION USING THIN FILM COATING

To achieve repulsive Casimir force or even stable levitation, let us consider the simplest configuration, i.e., two different substrates separated by a thin layer of fluid. Making the Casimir force repulsive is very challenging if the fluid is vacuum, however, it will be a different story for a fluid whose (relative) permittivity (or dielectric function) is ε_f. The repulsive Casimir force is readily achievable without exciting magnetic resonances as long as Dzyaloshinskii's condition: $\varepsilon_1(i\omega) < \varepsilon_f(i\omega) < \varepsilon_2(i\omega)$ is satisfied in a suitable frequency range. Here, ε_1 and ε_2 are the dielectric functions for the two nonmagnetic plates at the imaginary frequency [61]. Munday et al. [54] experimentally demonstrated repulsive Casimir force between gold and silica separated by bromobenzene whose permittivity lies between those of the two substrates for a broad frequency range, and their results agree with the general Lifshitz's formula for a wide range of gap distances [60]. When the fluid thickness is only a few nanometers where the retardation effects considering finite speed of light can be neglected, repulsive forces featured with negative Hamaker constant have also been experimentally demonstrated [64, 65]. Repulsive forces can lead to ultralow friction and good surface wetting [64, 66]. Some potential applications can be realized if the Casimir force can change sign with the distance. One such example is stable

quantum levitation [48, 49, 67], which can be used to design frictionless gears and develop passive-suspension techniques [4].

The requirement of stable levitation is that the Casimir interaction should be repulsive for small gap spacings and turns into an attractive force when the two objects move away from each other to a certain extent. If the Casimir interaction exhibits an opposite behavior, the state is dynamically instable though the magnitude of the force becomes zero at that transition position. To achieve stable separation between two bulk isotropic substrates, the following guide inequalities should be satisfied [67]

$$\begin{aligned} &\varepsilon_1 < \varepsilon_f < \varepsilon_2 \quad \text{at low frequencies} \\ &\varepsilon_f < \min\left(\varepsilon_1, \varepsilon_2\right) \text{ or } \varepsilon_f > \max\left(\varepsilon_1, \varepsilon_2\right) \text{ at high frequencies} \end{aligned} \tag{4}$$

It is not difficult to understand the above criteria since the low and high frequencies play a major role in determining the Casimir force for large and small gap distances, respectively. However, these criteria are only approximate and should be treated as guideline only [67]. Even if both inequalities in Eq. (4) are satisfied, it is not guaranteed that there will definitely be a stable position, since the contribution of different frequencies may vary largely. Therefore, realizing stable levitation based on proper choices of dielectric functions of the fluid and two bulk substrates is challenging though feasible for only a few delicately designed cases [67].

The three materials satisfying Eq. (4) selected in this work are a Si substrate, a bromobenzene fluid, and a Teflon substrate. The dielectric function of intrinsic Si is described by a Sellmeier model as [68]

$$\varepsilon_{\mathrm{Si}}\left(i\omega\right) = \varepsilon_\infty + \frac{\left(\varepsilon_0 - \varepsilon_\infty\right)\omega_0^2}{\omega^2 + \omega_0^2} \tag{5}$$

where the cutoff frequency ω_0 is equal to 6.6×10^{15} rad/s, ε_∞ and ε_0 are 11.87 and 1.035, respectively. For bromobenzene, a two-oscillator model is employed [54, 69]

$$\varepsilon_f(i\omega) = 1 + \frac{C_{\mathrm{IR}}\omega_{\mathrm{IR}}^2}{\omega^2+\omega_{\mathrm{IR}}^2} + \frac{C_{\mathrm{UV}}\omega_{\mathrm{UV}}^2}{\omega^2+\omega_{\mathrm{UV}}^2} \tag{6}$$

$\omega_{\mathrm{IR}} = 5.47\times10^{14}$ rad/s and $\omega_{\mathrm{UV}} = 1.286\times10^{16}$ rad/s are the characteristic absorption frequencies in the infrared and ultraviolet range, respectively, C_{IR} = 2.967 and C_{UV} = 1.335 are the corresponding absorption strengths. For Teflon, multiple oscillator models are used, the corresponding parameters obtained by combining Kramers-Kronig analysis and measured dielectric constants are given in a recent paper by van Zwol and Palasantzas [70]. The permittivities of these three materials at imaginary frequencies are shown in Fig. 2. It can be clearly seen that the permittivity of bromobenzene lies between that of Si and Teflon until the crossing frequency at 1.612×10^{16} rad/s. Although Eq. (4) is satisfied, as will be shown later, the Casimir force stays repulsive for all gap distances and stable levitation is not feasible with semi-infinite substrates.

Using multilayer structures such as a thin film coated on a substrate may facilitate stable levitation [49]. Here, the configuration of fluid bromobenzene sandwiched between intrinsic Si and a thin film of Teflon coated on Si substrate is considered, as shown in Fig. 3a. The Casimir force per unit area normalized to that between perfect conductors F_{c} for the considered planar configuration is shown in Fig. 3b for different thicknesses of Teflon. When the Teflon film thickness is zero, it recovers to the Si-bromobenzene-Si configuration. As expected, the Casimir force for this symmetric configuration as shown by the solid line is always attractive (positive sign) since r_1 is equal to r_2 for both polarizations. On the other hand, as shown by the dotted line, Casimir repulsion at all gap distances is supported for Si-bromobenzene-Teflon where Teflon

film thickness is infinitely large, although it is noted that Eq. (4) is satisfied with the transition frequency as 1.612×10^{16} rad/s, below and beyond which the spectral force becomes repulsive and attractive, respectively. The reason is because contributions from higher frequencies are relatively small compared with those from frequencies below the transition. Indeed, the permittivities of these three materials are very close and approach to unity at high frequencies as can be seen from Fig. 2. As a result, the field confinement in the gap becomes weak, leading to small Casimir interactions. When the Teflon film thickness is finite, say 50 nm, the Casimir force lies between the above two limiting cases of pure attraction and pure repulsion, as illustrated by the dashed line. Stable position with diminishing force occurs at 195.2 nm as denoted by the solid circle, and the sign becomes positive and negative by further increasing and decreasing the gap spacing, respectively. Fig. 3b shows that the Casimir force considering thin film Teflon of 50 nm approaches the force for bulk Teflon (repulsion) and bulk Si (attraction) at small and large gap distances, respectively. Given this situation, there should be a middle point at which the transition occurs. In order to elucidate this phenomenon, it is necessary to take a look at the reflection coefficient for the thin Teflon coating on bulk Si, which is given as [63]

$$r_2^{\mathrm{s,p}} = \frac{r_{\text{Br-Te}}^{\mathrm{s,p}} + r_{\text{Te-Si}}^{\mathrm{s,p}} e^{-2k_{z,\mathrm{Te}}H_2}}{1 + r_{\text{Br-Te}}^{\mathrm{s,p}} r_{\text{Te-Si}}^{\mathrm{s,p}} e^{-2k_{z,\mathrm{Te}}H_2}} \tag{7}$$

where $k_{z,\mathrm{Te}} = \sqrt{\varepsilon_{\mathrm{Te}}\,\omega_n^2/c^2 + \beta^2}$ is the z-direction wavevector in Teflon, $r_{\text{Br-Te}}$ and $r_{\text{Te-Si}}$ are the Fresnel reflection coefficients are the interface of bromobenzene-Teflon and Teflon-Si, respectively. At high frequencies, $k_{z,\mathrm{Te}}$ becomes so large that $e^{-2k_{z,\mathrm{Te}}H_2}$ will approach zero, then $r_2 \approx r_{\text{Br-Te}}$. This means that the underlying Si substrate will not affect the reflection coefficient, and the thin Teflon film can be treated as bulk although its thickness is finite with the value of H_2. That explains the overlap of the Casimir force considering Teflon of 50 nm and that for bulk

Teflon at gap distances smaller than 20 nm, as can be clearly seen from Fig. 3b. At low frequencies, relatively small $k_{z,\mathrm{Te}}$ multiplies with nanometer scale H_2 will make $e^{-2k_{z,\mathrm{Te}}H_2}$ close to one. After some math work, it can be found that $r_2 \approx r_{\mathrm{Br\text{-}Si}}$, meaning that the existence of thin Teflon film will not lead to a large modification of the Casimir force between bulk Si substrates at large gap distances, where the Casimir force is dominated by low frequencies. Therefore, thin film coatings can help achieve stable levitation.

The stable separation distance can be adjusted by changing the thickness of Teflon film as shown in Fig. 3c. The stable position decreases with reducing Teflon thickness, and the separation is 6.3 nm when H_2 is 5 nm. When Teflon thickness becomes larger, the deviation of the corresponding Casimir force from that of bulk Teflon will be postponed to larger gap distances. On the other hand, the gap spacing needed to make the substrate effects large enough to achieve attraction should increase. This is why the stable levitation position increases monotonically with the thickness of Teflon. Nevertheless, the adjustment of stable separation is based on changing Teflon film thickness and cannot be made on-site or dynamically to meet different requirements of various applications. The above limitation can be overcome by the proposed design shown in Fig. 1 and the details are given in the next section.

IV. DYNAMIC TUNABILITY BASED ON LATERAL DISPLACEMENT

The Casimir force between Si grating and Teflon grating as a function of the fluid gap distance is given in Fig. 4. Here, P = 1000 nm, W = 500 nm, L = 0 nm, and H_2 = 50 nm are set as default unless otherwise specified. The agreement between the exact method represented by marks and PFA denoted by the dash or dotted line is good for different values of H_1. Stable separation occurs at 125.6 nm and 115.7 nm for H_1 equal to 50 nm and 30 nm, respectively.

These values agree with 136.6 nm and 122.9 nm obtained from PFA to some extent. For small gap distances, the Casimir force at two different values of H_1 coincides, as is confirmed from both the exact method and PFA. It is expected since the contribution to the force from the ridges (Si and Teflon) becomes more dominant over that from the grooves (Si and Si) with decreasing d. This is essentially due to the power law dependence of Casimir force on the gap spacing. Though variations of H_1 do not affect the Casimir interaction for small d, an apparent difference occurs for relatively large d. Decreasing H_1 will increase the attractive force between the grooves, while the repulsive force between the ridges remains the same. In order to balance the increased attractive force, the gap spacing has to be reduced to produce enough repulsion from the ridges. As a result, the stable levitation position shifts from 125.6 nm to 115.7 nm when decreasing H_1 from 50 nm to 30 nm. The equilibrium position can also be modified by changing H_2 and W.

As shown in Fig. 5a, the stable levitation position at W = 500 nm, H_1 = 30 nm, and H_2 = 50 nm, decreases with the lateral displacement between the top and bottom gratings. In the present study, lateral Casimir force is not considered although it exists for misaligned cases except when the lateral shift is half of the period due to symmetry. It is assumed that the lateral shift is controlled externally. The curve is symmetric with respect to $L = 0.5P$; as such the other half period for L = 500 nm to 1000 nm is not drawn. With increasing the lateral displacement, the dominant repulsion force from the ridges of the two gratings will decrease since the facing area becomes smaller while the dominant attraction force from the ridge of the top grating to the groove of the bottom grating increases. Subsequently, the separation distance for stable levitation will decrease. The agreement between the exact method and PFA is excellent except for the two extreme cases of L = 0 nm and L = 500 nm. PFA overestimates and underestimates the equilibrium position when L is close to 0 nm and 500 nm, respectively. The reason lies that PFA

does not consider the edge effects. For example, when L = 0 nm, according to PFA, the equilibrium is settled when the repulsion force between the ridges and the attraction force between the grooves are equal. However, the field confinement between the ridges cannot be as perfect as that between bulks, so that the real repulsion will be smaller than the PFA value due to the leakage. This explains why the exact values of Casimir force are all above the PFA curves in Fig. 4. Then, there is no wondering that the PFA predicts a larger stable separation for aligned gratings. For the purely misaligned case of L = 500 nm, balance of the repulsion from the groove of the top grating and the ridge of the bottom grating with the attraction from the corresponding remaining parts leads to the equilibrium position. However, the repulsion between the ridges, which is nontrivial especially for small gap distances, is not considered by PFA. As a result, the exact values of Casimir force will lie below the PFA predictions although the results are not shown here. This explains why the stable separation predicted by PFA, 15.4 nm, is smaller than the exact value of 35.7 nm at L = 500 nm. Nevertheless, the overall accuracy of PFA is still good except close to the two extremes. If the period is large enough, the edge effects are expected to diminish, and the accuracy of PFA will further improve.

It is clearly shown that by laterally moving the bottom grating relative to the top one, the stable levitation position can be tuned on-site. It is noted that both the magnitude of the vertical displacement and its shape can be adjusted to meet different demands by changing the ridge width W. The equilibrium position varying with the lateral displacement for W = 300 nm is given in Fig. 5b. The stable separation first decreases with L, as expected, and reaches a constant for L larger than 300 nm. This provides rich vertical motions, which might be useful for different applications. The maximum vertical displacement induced when L changes from 0 to 300 nm is 73.1 nm, which is slightly smaller than 79.9 nm in Fig. 5a. The stable position in Fig. 5b for W =

300 nm is lower than that in Fig. 5a for any value of the later shift. It is expected since the reducing W will decrease the repulsion between the ridges but enlarge the attraction between the grooves. Besides the conventional applications for stable levitation, the proposed design can be used as for position control. It can also work as mechanical transducers by converting lateral displacement into motion in the vertical direction. Instead of relying on classical mechanics or electromagnetism, this envisioned device is based on quantum electrodynamics, and no contact is required so that the friction is expected to be ultralow. The ratio of maximum vertical displacement to the lateral shift is inversely proportional to the period, thus can be tuned to meet different needs. Besides, the device size can be scalable from macroscale down to microscale. Another advantage of the proposed configuration is that the alignment of the two gratings can be self-acquired to some extent. If a certain misalignment is introduced, the Casimir force will be repulsive and attractive for regimes with smaller and larger gap separations, respectively. As a result, the gap distance between the two gratings would tend to approach the same value across the whole sample.

V. Effects of Temperature and Gravity

In practice, the effects of temperature and gravity on the stable position should also be considered. The effect of thermal fluctuations may be nontrivial for bulk materials when the gap spacing is on the order of $\hbar c/k_B T$, which is 7.6 μm at T = 300 K [60]. Around room temperature, modifications of the Casimir force due to temperature changes are typically negligible [71]. However, Guérout et al. [28] found that the grating structure could augment the thermal contribution to the Casimir interactions. Therefore, it is necessary to check the sensitivity of proposed device to temperature changes. The liquid phase of fluid bromobenzene holds when the

temperature is between 242.3 K and 429 K at atmospheric pressure. Since the stable separation distance is around 100 nm, the Casimir force is calculated for aligned gratings with default geometric parameters at d = 100 nm for T = 250 K and 420 K. The relative difference is only three percent, demonstrating that the temperature has a negligible effect on the Casimir force. The stable position for L = 0 nm changes slightly from 115.66 nm to 115.57 nm when the temperature increases from 250 K to 420 K. It should be noted that according to the PFA, the stable position is changed from 122.97 nm to 122.55 nm, which qualitatively agree with the exact calculations. Therefore, it is safe to assert that the stable levitation of proposed nanostructures is robust to temperature variations.

The gravitational force generally needs to be considered for application with the proposed configuration shown in Fig. 1, although when the z axis lies horizontally, gravity will not have an effect on the preceding results. In order to consider the gravitational effect, it is assumed that the top grating is beneath a thin Si film with a thickness H_{Si} of 5 μm. The medium above the Si film is vacuum. Taking the gravitational acceleration rate g = 9.8 m/s^2, the density of Si ρ_{Si} = 2329 kg/m^3, and the density of BB ρ_{BB} = 1492 kg/m^3, the force per unit area exerted on the top grating due to gravity is $F_g = \rho_{\mathrm{Si}} g H_{\mathrm{Si}} + \rho_{\mathrm{Si}} g H_1 f - \rho_{\mathrm{BB}} g H_1 f$. The last term considers the buoyancy of the grooves immersed in the fluid. For default geometry parameters, i.e., P = 1000 nm, W = 500 nm, H_1 = 30 nm, and H_2 = 50 nm, F_{g} is equal to 0.11424 Pa. So, the Casimir force between the two nanostructures should be repulsive and the magnitude should be equal to F_{g} for stable levitation in the presence of gravity. As can be seen from Fig. 4, the Casimir force is always repulsive when the gap distance is smaller than the original stable levitation separation. Therefore, the stable levitation considering the gravity still exists but will shift to a smaller gap separation for the balance of gravitational force with the repulsive Casimir force.

Figure 6 is given to illustrate the gravity effect on the variation of the stable levitation position of the top grating with the thin Si substrate. Clearly, the stable separation distance is always smaller than the case without gravity for different values of lateral shifts as expected. Another prominent feature of Fig. 6 is that the difference of the stable levitation separation with or without gravity becomes smaller as the lateral shift increases. Note that the stable levitation gap distance is smaller at a larger lateral shift. Because the Casimir force is very sensitive to the gap distance when it is small, even a tiny further decrease of the gap distance will lead to a repulsive Casimir force comparable to the gravitational force. As shown in Fig. 6, for L equal to 500 nm, there is only a small decrease in the stable levitation separation.

V. CONCLUSION

The Casimir interaction between two nanostructures separated by an intervening fluid is investigated. While stable levitation is achievable when one substrate and a thin film coated on another substrate are separated by a non-vacuum fluid, the levitation position depending on the film thickness is fixed rather than actively tunable. This limitation can be overcome by using dissimilar gratings, whereby the stable separation position changes when the two gratings move relative to each other laterally. Besides, how the levitation position changes with the lateral shift depends on the grating width. Thus, the grating width can be adjusted to meet different applications. In addition, the position of stable levitation is insensitive to temperature variations. This work opens new possibilities to turn quantum Casimir force into real applications in macroscopic devices, which include but are not limited to position control and mechanical transduction.

Acknowledgements

This work was mainly supported by the US Department of Energy, Office of Science, Basic Energy Sciences (DE-FG02-06ER46343), and ZMZ also thanks the support by the National Science Foundation (CBET-1235975).

References

[1] H.B.G. Casimir, Proc. K. Ned. Akad. Wet. **51**, 793 (1948).

[2] G. L. Klimchitskaya, U Mohideen, and V. M Mostepanenko, The Casimir force between real materials: experiment and theory, Rev. Mod. Phys. **81**, 1827 (2009).

[3] Alejandro W Rodriguez, Federico Capasso, and Steven G Johnson, The Casimir effect in microstructured geometries, Nat. Photon. **5**, 211-221 (2011).

[4] F. Capasso, J. N. Munday, D. Iannuzzi, and H. B. Chan, Casimir Forces and Quantum Electrodynamical Torques: Physics and Nanomechanics, IEEE J. Sel. Top. Quantum Electron. **13**, 400-414 (2007).

[5] C. Genet, A. Lambrecht, and S. Reynaud, The Casimir effect in the nanoworld, Eur. Phys. J. Spec. Top. **160**, 183-193 (2008).

[6] Diego Dalvit, Peter Milonni, David Roberts, and Felipe da Rosa, Casimir Physics (Springer, 2011).

[7] Michael Bordag, Galina Leonidovna Klimchitskaya, Umar Mohideen, and Vladimir Mikhaylovich Mostepanenko, Advances in the Casimir effect (Oxford University Press, 2009).

[8] K. Joulain, J. P. Mulet, F. Marquier, R. Carminati, and J. J. Greffet, Surface electromagnetic waves thermally excited: Radiative heat transfer, coherence properties and Casimir forces revisited in the near field, Surf. Sci. Rep. **57**, 59-112 (2005).

[9] H. B. Chan, Y. Bao, J. Zou, R. A. Cirelli, F. Klemens, W. M. Mansfield, and C. S. Pai, Measurement of the Casimir Force between a Gold Sphere and a Silicon Surface with Nanoscale Trench Arrays, Phys. Rev. Lett. **101**, 030401 (2008).

[10] Y Bao, R Guérout, J Lussange, A Lambrecht, R. A Cirelli, F Klemens, W. M Mansfield, CS Pai, and H. B Chan, Casimir force on a surface with shallow nanoscale corrugations: Geometry and finite conductivity effects, Phys. Rev. Lett. **105**, 250402 (2010).

[11] J. Zou, Z. Marcet, A. W. Rodriguez, M. T. H. Reid, A. P. McCauley, I. I. Kravchenko, T. Lu, Y. Bao, S. G. Johnson, and H. B. Chan, Casimir forces on a silicon micromechanical chip, Nat Commun. **4**, 1845 (2013).

[12] Francesco Intravaia, Stephan Koev, Il Woong Jung, A. Alec Talin, Paul S. Davids, Ricardo S. Decca, Vladimir A. Aksyuk, Diego A. R. Dalvit, and Daniel López, Strong Casimir force reduction through metallic surface nanostructuring, Nat. Commun. **4**, (2013).

[13] Astrid Lambrecht and Valery N. Marachevsky, Casimir Interaction of Dielectric Gratings, Phys. Rev. Lett. **101**, 160403 (2008).

[14] Giuseppe Bimonte, Thorsten Emig, and Mehran Kardar, Casimir-Polder interaction for gently curved surfaces, Phys. Rev. D **90**, 081702 (2014).

[15] Alejandro Rodriguez, Alexander McCauley, John Joannopoulos, and Steven Johnson, Casimir forces in the time domain: Theory, Phys. Rev. A **80**, 012115 (2009).

[16] X. L. Liu, Bo Zhao, and Zhuomin M. Zhang, Enhanced near-field thermal radiation and reduced Casimir stiction between doped-Si gratings, Phys. Rev. A **91**, 062510 (2015).

[17] H-C Chiu, G. L. Klimchitskaya, V. N. Marachevsky, V. M. Mostepanenko, and U Mohideen, Demonstration of the asymmetric lateral Casimir force between corrugated surfaces in the nonadditive regime, Phys. Rev. B **80**, 121402 (2009).

[18] H-C Chiu, G. L. Klimchitskaya, V. N. Marachevsky, V. M. Mostepanenko, and U Mohideen, Lateral Casimir force between sinusoidally corrugated surfaces: Asymmetric profiles, deviations from the proximity force approximation, and comparison with exact theory, Phys. Rev. B **81**, 115417 (2010).

[19] AA Banishev, J Wagner, T Emig, R Zandi, and U Mohideen, Demonstration of Angle-Dependent Casimir Force between Corrugations, Phys. Rev. Lett. **110**, 250403 (2013).

[20] A. A Banishev, J Wagner, T Emig, R Zandi, and U Mohideen, Experimental and theoretical investigation of the angular dependence of the Casimir force between sinusoidally corrugated surfaces, Phys. Rev. B **89**, 235436 (2014).

[21] D. Drosdoff and Lilia M. Woods, Quantum and Thermal Dispersion Forces: Application to Graphene Nanoribbons, Phys. Rev. Lett. **112**, 025501 (2014).

[22] M. Bordag, G. L. Klimchitskaya, and V. M. Mostepanenko, Thermal Casimir effect in the interaction of graphene with dielectrics and metals, Phys. Rev. B **86**, 165429 (2012).

[23] S. A. Biehs and G. S. Agarwal, Anisotropy enhancement of the Casimir-Polder force between a nanoparticle and graphene, Phys. Rev. A **90**, 042510 (2014).

[24] A. I. Volokitin and B. N. J. Persson, Influence of electric current on the Casimir forces between graphene sheets, Europhys. Lett. **103**, 24002 (2013).

[25] G. L. Klimchitskaya, V. M. Mostepanenko, and Bo E. Sernelius, Two approaches for describing the Casimir interaction in graphene: Density-density correlation function versus polarization tensor, Phys. Rev. B **89**, 125407 (2014).

[26] Bo E Sernelius, Casimir effects in systems containing 2D layers such as graphene and 2D electron gases, J. Phys.: Condens. Matter **27**, 214017 (2015).

[27] A. O Sushkov, W. J Kim, D. A. R Dalvit, and S. K Lamoreaux, Observation of the thermal Casimir force, Nature Phys. **7**, 230 (2011).

[28] R. Guérout, J. Lussange, H. B. Chan, A. Lambrecht, and S. Reynaud, Thermal Casimir force between nanostructured surfaces, Phys. Rev. A **87**, 052514 (2013).

[29] Iver Brevik and Johan S Høye, Temperature dependence of the Casimir force, Eur. J. Phys. **35**, 015012 (2014).

[30] R. S. Decca, D López, E Fischbach, G. L. Klimchitskaya, D. E. Krause, and V. M. Mostepanenko, Novel constraints on light elementary particles and extra-dimensional physics from the Casimir effect, Eur. Phys. J. C **51**, 963 (2007).

[31] C-C Chang, A. A Banishev, R Castillo-Garza, G. L. Klimchitskaya, V. M. Mostepanenko, and U Mohideen, Gradient of the Casimir force between Au surfaces of a sphere and a plate

measured using an atomic force microscope in a frequency-shift technique, Phys. Rev. B **85**, 165443 (2012).

[32] A. A Banishev, G. L. Klimchitskaya, V. M. Mostepanenko, and U Mohideen, Demonstration of the Casimir force between ferromagnetic surfaces of a Ni-coated sphere and a Ni-coated plate, Phys. Rev. Lett. **110**, 137401 (2013).

[33] Timothy Boyer, Van der Waals forces and zero-point energy for dielectric and permeable materials, Phys. Rev. A **9**, 2078-2084 (1974).

[34] O. Kenneth, I. Klich, A. Mann, and M. Revzen, Repulsive Casimir Forces, Phys. Rev. Lett. **89**, 033001 (2002).

[35] F. S. S. Rosa, D. A. R. Dalvit, and P. W. Milonni, Casimir-Lifshitz Theory and Metamaterials, Phys. Rev. Lett. **100**, 183602 (2008).

[36] R. Zhao, J. Zhou, Th Koschny, E. Economou, and C. Soukoulis, Repulsive Casimir Force in Chiral Metamaterials, Phys. Rev. Lett. **103**, 103602 (2009).

[37] Venkatesh K. Pappakrishnan, Pattabhiraju C. Mundru, and Dentcho A. Genov, Repulsive Casimir force in magnetodielectric plate configurations, Phys. Rev. B **89**, 045430 (2014).

[38] Yaping Yang, Ran Zeng, Jingping Xu, and Shutian Liu, Casimir force between left-handed-material slabs, Phys. Rev. A **77**, 015803 (2008).

[39] Leonhardt Ulf and G. Philbin Thomas, Quantum levitation by left-handed metamaterials, New J. Phys. **9**, 254 (2007).

[40] Pablo Rodriguez-Lopez and Adolfo G Grushin, Repulsive Casimir effect with Chern insulators, Phys. Rev. Lett. **112**, 056804 (2014).

[41] X. L. Liu, T. J. Bright, and Z. M. Zhang, Application conditions of effective medium theory in near-field radiative heat transfer between multilayered metamaterials, J. Heat Transfer **136**, 092703 (2014).

[42] Alexander McCauley, Rongkuo Zhao, M. Reid, Alejandro Rodriguez, Jiangfeng Zhou, F. Rosa, John Joannopoulos, D. Dalvit, Costas Soukoulis, and Steven Johnson, Microstructure effects for Casimir forces in chiral metamaterials, Phys. Rev. B **82**, 165108 (2010).

[43] B Geyer, G. L. Klimchitskaya and V. M. Mostepanenko, Thermal Casimir interaction between two magnetodielectric plates, Phys. Rev. B **81**, 104101 (2010).

[44] Mauro Antezza, Lev P Pitaevskii, and Sandro Stringari, New asymptotic behavior of the surface-atom force out of thermal equilibrium, Phys. Rev. Lett. **95**, 113202 (2005).

[45] Sahand Jamal Rahi, Mehran Kardar, and Thorsten Emig, Constraints on stable equilibria with fluctuation-induced (Casimir) forces, Phys. Rev. Lett. **105**, 070404 (2010).

[46] Michael Levin, Alexander P McCauley, Alejandro W Rodriguez, MT Homer Reid, and Steven G Johnson, Casimir repulsion between metallic objects in vacuum, Phys. Rev. Lett. **105**, 090403 (2010).

[47] Matthias Krüger, Giuseppe Bimonte, Thorsten Emig, and Mehran Kardar, Trace formulas for nonequilibrium Casimir interactions, heat radiation, and heat transfer for arbitrary objects, Phys. Rev. B **86**, 115423 (2012).

[48] Alejandro Rodriguez, J. Munday, J. Joannopoulos, Federico Capasso, Diego Dalvit, and Steven Johnson, Stable Suspension and Dispersion-Induced Transitions from Repulsive Casimir Forces Between Fluid-Separated Eccentric Cylinders, Phys. Rev. Lett. **101**, 190404 (2008).

[49] Maofeng Dou, Fei Lou, Mathias Boström, Iver Brevik, and Clas Persson, Casimir quantum levitation tuned by means of material properties and geometries, Phys. Rev. B **89**, 201407 (2014).

[50] Anh D Phan, Lilia M Woods, D Drosdoff, IV Bondarev, and NA Viet, Temperature dependent graphene suspension due to thermal Casimir interaction, Appl. Phys. Lett. **101**, 113118 (2012).

[51] Norio Inui, Levitation of a metallic sphere near gas-liquid and liquid-liquid interfaces by the repulsive Casimir force, Phys. Rev. A **89**, 062506 (2014).

[52] G. L. Klimchitskaya, U Mohideen, and V. M Mostepanenko, Pulsating Casimir force, J. Phys. A: Math. Theor. **40**, F841 (2007).

[53] BW Ninham and VA Parsegian, Van der Waals interactions in multilayer systems, J. Chem. Phys. **53**, 3398 (1970).

[54] Jeremy N Munday, Federico Capasso, and V Adrian Parsegian, Measured long-range repulsive Casimir–Lifshitz forces, Nature **457**, 170 (2009).

[55] VA Parsegian and BW Ninham, Application of the Lifshitz theory to the calculation of van der Waals forces across thin lipid films, Nature **224**, 1197 (1969).

[56] X. L. Liu and Z. M. Zhang, Graphene-assisted near-field radiative heat transfer between corrugated polar materials, Appl. Phys. Lett. **104**, 251911 (2014).

[57] X. L. Liu and Z. M. Zhang, Giant enhancement of nanoscale thermal radiation based on hyperbolic graphene plasmons, Appl. Phys. Lett. **107**, 143114 (2015).

[58] Xianglei Liu and Zhuomin Zhang, Near-field thermal radiation between metasurfaces, ACS Photon. **2**, 1320 (2015).

[59] J. Lussange, R. Guérout, F. S. S. Rosa, J. J. Greffet, A. Lambrecht, and S. Reynaud, Radiative heat transfer between two dielectric nanogratings in the scattering approach, Phys. Rev. B **86**, 085432 (2012).

[60] E. M. Lifshitz, The theory of molecular attractive forces between solids, Sov. Phys. JETP **2**, 73 (1956).

[61] I. E. Dzyaloshinskii, E. M. Lifshitz, and L. P. Pitaevskii, The general theory of van der Waals forces, Adv. Phys. **10**, 165 (1961).

[62] Yi Zheng and Arvind Narayanaswamy, Lifshitz theory of van der Waals pressure in dissipative media, Phys. Rev. A **83**, 042504 (2011).

[63] Z. M. Zhang, Nano/Microscale Heat Transfer (McGraw-Hill, New York, 2007).

[64] Adam A. Feiler, Lennart Bergström, and Mark W. Rutland, Superlubricity Using Repulsive van der Waals Forces, Langmuir **24**, 2274 (2008).

[65] Seung-woo Lee and Wolfgang M Sigmund, AFM study of repulsive van der Waals forces between Teflon AF™ thin film and silica or alumina, Colloids Surf. A **204**, 43 (2002).

[66] Michael Elbaum and M Schick, Application of the theory of dispersion forces to the surface melting of ice, Phys. Rev. Lett. **66**, 1713 (1991).

[67] Alejandro Rodriguez, Alexander McCauley, David Woolf, Federico Capasso, J. Joannopoulos, and Steven Johnson, Nontouching Nanoparticle Diclusters Bound by Repulsive and Attractive Casimir Forces, Phys. Rev. Lett. **104**, 160402 (2010).

[68] I Pirozhenko and A Lambrecht, Influence of slab thickness on the Casimir force, Phys. Rev. A **77**, 013811 (2008).

[69] Andrew Milling, Paul Mulvaney, and Ian Larson, Direct Measurement of Repulsive van der Waals Interactions Using an Atomic Force Microscope, J. Colloid Interface Sci. **180**, 460 (1996).

[70] P. van Zwol and G. Palasantzas, Repulsive Casimir forces between solid materials with high-refractive-index intervening liquids, Phys. Rev. A **81**, 062502 (2010).

[71] Alejandro Rodriguez, David Woolf, Alexander McCauley, Federico Capasso, John Joannopoulos, and Steven Johnson, Achieving a Strongly Temperature-Dependent Casimir Effect, Phys. Rev. Lett. **105**, 060401 (2010).

Figure Captions:

FIG. 1 Schematic of Casimir interaction between one-dimensional gratings of dissimilar materials with a separation gap distance of d immersed in fluid bromobenzene. P is the period, W is the grating width, and L is the lateral shift. H_1 and H_2 are the depth of Si grating and Teflon grating, respectively. All objects are assumed to be in thermal equilibrium at temperature T.

FIG. 2 Relative permittivity of Si, bromobenzene, and Teflon at imaginary frequencies.

FIG. 3 (a) The configuration of Casimir interaction between bulk Si and thin film Teflon deposited on Si substrate. (b) Normalized Casimir force as a function of the gap spacing for different bottom configurations: bulk Si, thin Teflon of 50 nm on Si, and bulk Teflon. The solid circle represents the stable separation point. (c) The variation of stable levitation position versus the thickness of Teflon film.

FIG. 4 Normalized Casimir force between grating structures varying with gap distances based on both exact method (marks) and PFA (lines). Two different depths of top Si grating of 30 nm and 50 nm are used, which are denoted as triangles pointing down and up, respectively.

FIG. 5 Stable levitation position tuned by the lateral displacement for different grating widths. (a) W = 500 nm; (b) W = 300 nm.

FIG. 6 Effect of the gravity on the tunable levitation when the top grating is attached to a thin Si substrate, H_{Si} = 5 μm, and the other geometry parameters are default.

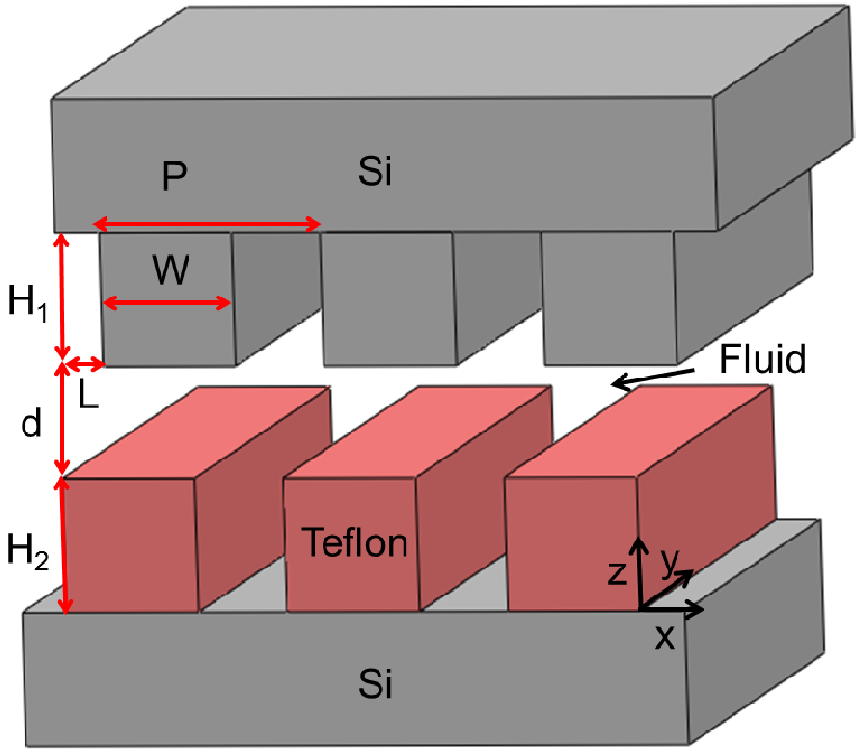

Liu and Zhang, Fig. 1

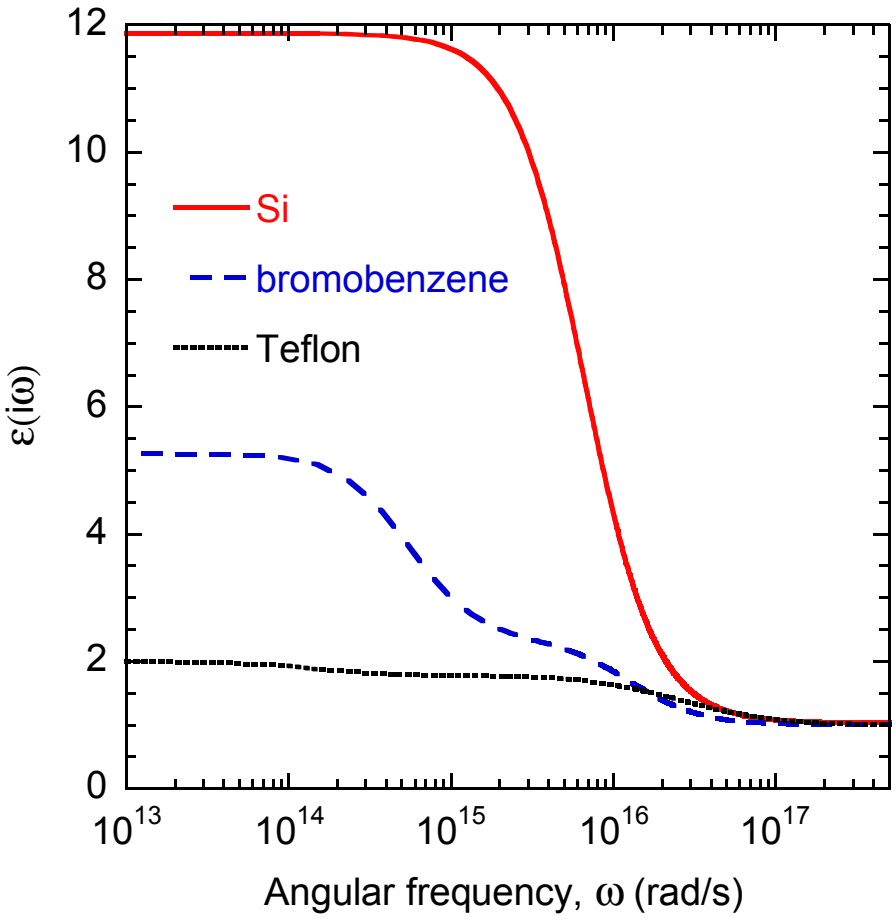

Liu and Zhang, Fig. 2

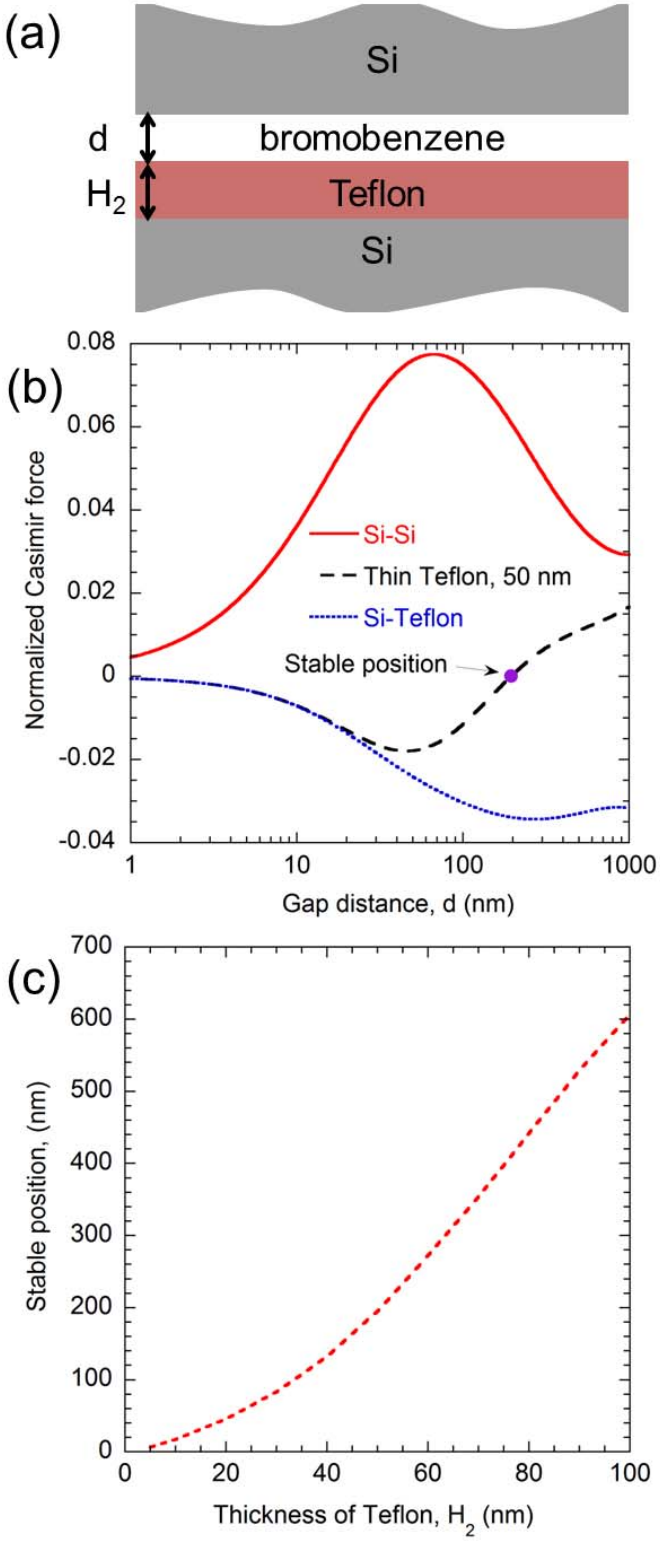

Liu and Zhang, Fig. 3

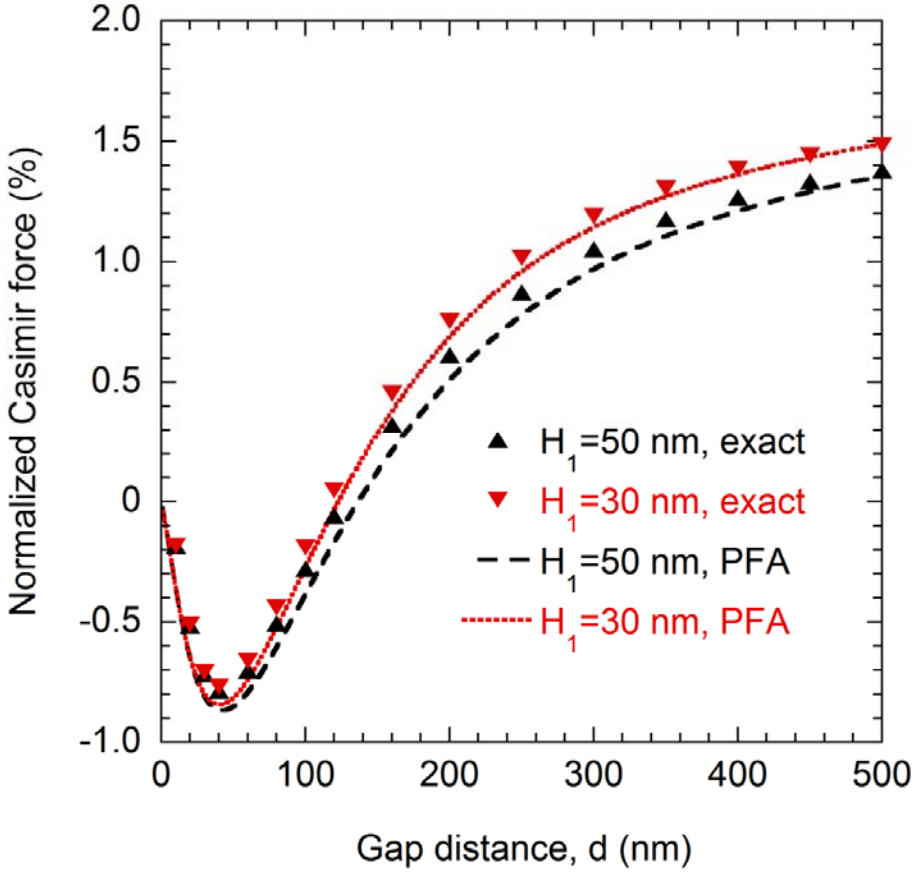

Liu and Zhang, Fig. 4

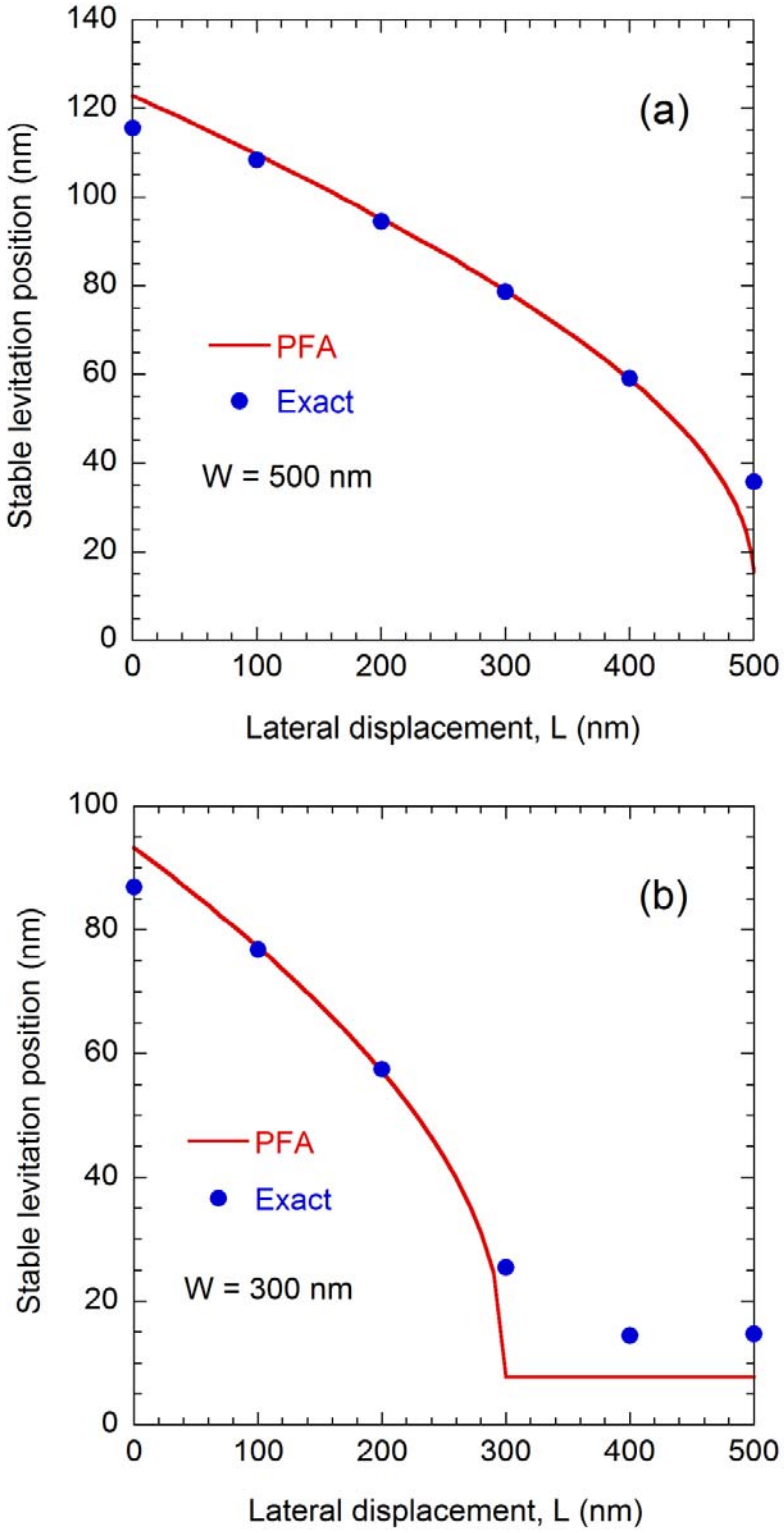

Liu and Zhang, Fig. 5

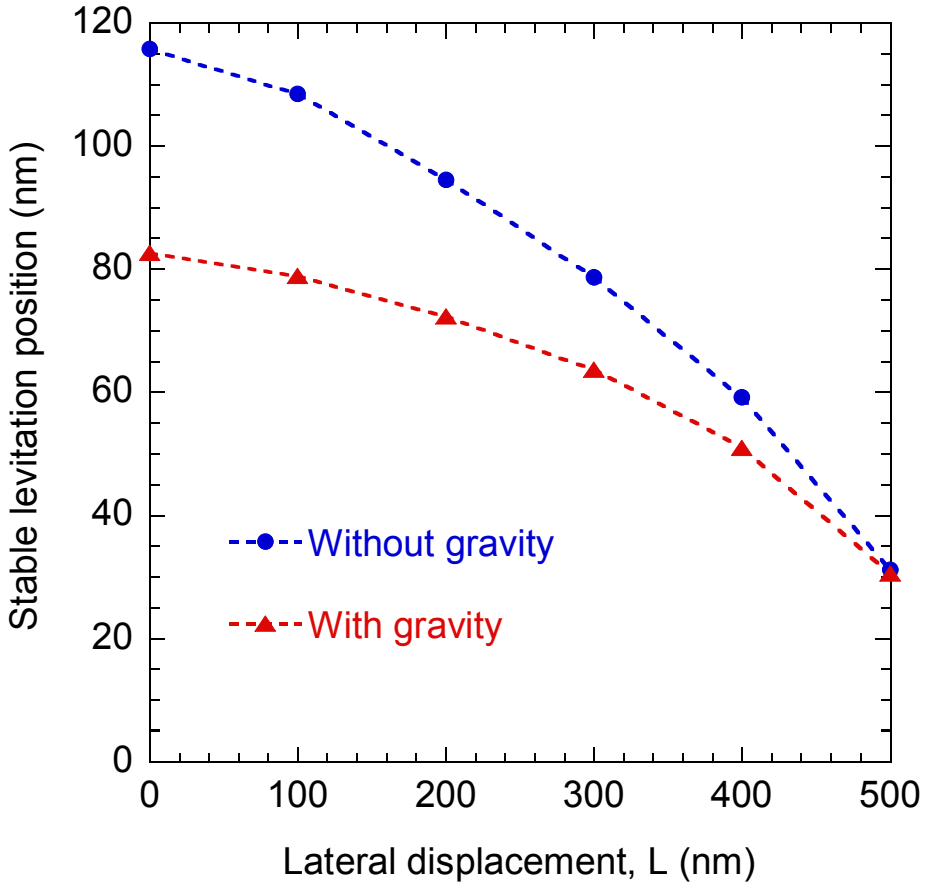

Liu and Zhang, Fig. 6